Journal of the European Ceramic Society 22 (2002) 613–623

www.elsevier.com/locate/jeurceramsoc

Effect of sintering temperature on functional properties of alumina membranes

Erkki Levänen*, Tapio Mäntylä

Institute of Materials Science, Tampere University of Technology, PO Box 589, FIN-33101 Tampere, Finland

Received 14 September 2000; received in revised form 10 May 2001; accepted 20 May 2001

Abstract

Supported membranes were prepared from different submicron alumina powders. The evolution of pore size, hardness and permeability were monitored after sintering the films at temperatures ranging from 1000 to 1400 °C. These functional properties and the microstructure of the films were compared with the free-standing membranes. Sintering at temperature range from 1000 to 1200 °C maintained the narrow, monomodal pore size distribution of the supported membranes. The effect of sintering temperature on the hardness of the membranes was weak. The permeability was also independent on the sintering temperature. When sintering temperature was raised up to 1300 and 1400 °C, the pore size increased significantly and distribution was changed to bimodal containing fraction of large pores. The hardness of the membranes increased while significant densification was not observed. Permeability increased due to the large pore size and the high porosity. In sintering of the free-standing membranes pore size remained almost unchanged, density increased when sintering temperature was raised, hardness was dependent on the density and permeability decreased continuously. The substrate did not have effect on the grain growth, which was dependent on the sintering temperature. Evolution of the properties of the free-standing membranes suggests local densification. The rigid substrate restricts the sintering shrinkage leading to densification of small areas. This local densification opens large flow channels between agglomerates. This increases the pore size, broadens the pore size distribution and increases the permeability. The macroscopic densification of the film is small.

Keywords: Al_2O_3; Membranes; Microstructure-final; Porosity; Sintering

1. Introduction

The ceramic membranes usually consist of several layers. Coarse pore sized, thick substrate gives strength to the structure. One or several thin intermediate layers exist on the substrate reducing the pore size towards that of the top separation layer. The pore size of the top-layer is selected according to the requirements of the application. The multi-layered structure combines small pore size with high permeability. The layers on the substrate are usually prepared by colloidal route from slips by packing of dispersed particles. The parameters of colloidal processing and their effect on the final structure have been studied widely.[1–4]

The preparation of the multi-layered ceramic membrane consists of several sintering cycles.[5–7] After deposition of each layer it is sintered at temperatures lower than the sintering temperature of the previous layer. The previously sintered structure acts as rigid substrate allowing the finer layer to shrink only in the direction perpendicular to the surface. This restriction leads to differences in densification and properties compared with the free-standing structure.

The use of multi-layered structures has focused the interest in the sintering of the constrained particulate film on a rigid support.[8–13] Bordia and Raj[8] have modelled the stresses developing during sintering of constrained particulate film. Their model is based on the assumption that the film is linear viscoelastic solid with spherical isolated pores. They found that if the shear rate, caused by densification and the resisting substrate, develops faster than the material can respond by relaxation, high tensile stresses may occur. These stresses are developed during the initial stages of sintering. The neck size is still small and stresses may lead to the formation of defects. The defect may be a brittle crack caused by the elastic strain energy or a crack grown by

* Corresponding author.
E-mail address: erkki.levanen@tut.fi (E. Levänen).

0955-2219/02/$ - see front matter
PII: S0955-2219(01)00334-X

time dependent diffusional growth of pores. The crack formation can be avoided with large particle size and high sintering temperature. The large particle size anyhow reduces the densification rate. The small particle size favours the defect formation and the substrate reduces the densification rate. Garino and Bowen[9,10] studied the densification kinetics of the particulate film in the case of viscous sintering, liquid phase sintering and solid state sintering. They assumed material as a viscous continuum. In the case of viscous sintering the model described well the densification of constrained film. The solid state sintering led to significantly lower density than predicted by the model. The grain growth alone did not explain the low density. Lower density was explained by the anisotropy during sintering resulting in the dense regions separated by the porous regions. Carroll and Rahaman[11] used the data of Garino and Bowen for testing a model, based on the cubic packing of spherical particles. Their model assumed that the material is transported from the top and the bottom necks to the side necks of the particles. They found that the densification rate of the constrained thin films is highly dependent on the dihedral angle of the material and on the grain growth. The grain growth can essentially stop the film from densifying.

Microstructural evolution in films of nanosized particles, especially titania, have been widely studied.[14–18] These studies have been focused on the densification, on the evolution of pore size and permeability, and on the effect of the substrate on the phase transformation temperature. These studies confirm that the substrate restricts the densification and the porosity decreases at higher temperatures compared with the free-standing films. The grain and pore size either increased or decreased probably depending on the particle coordination number. The local densification resulted on a strong grain growth. When the pore size increased the permeability usually increased, but the permeability data was not always available. The substrate typically increased the phase transformation temperature for the materials such as anatase–rutile transformation for titania. These papers anyhow concentrated on the microstructural evolution of the nanoparticle sized supported films and the study of the functional properties was not deeply concerned.

These models and studies describe the densification of particulate structure. However, the information from the evolution of the functional properties is also needed, since pore size, permeability and hardness are usually the properties that define the suitability of the membrane for planned application. This paper concentrates on the effect of sintering temperature on the properties of both the free-standing films and the supported films. The evolution of properties such as pore size, pore size distribution, hardness and permeability are followed and compared with the respective microstructure. The microstructural analysis is used for explaining the found differences between properties of the free-standing and the supported films.

2. Experimental

2.1. Materials

Free-standing films and supported films were prepared from three commercial submicron α-alumina powders (Alcoa 16 SG, Alcoa Industrial Chemicals Europe, Bad Homburg, Germany, Baikalox CR 6, Baikowski International Corporation, Charlotte, NC, USA, and AKP-30, Sumitomo Chemical Co., Ltd., Tokyo, Japan). Powders were dispersed into de-ionised water with nitric acid. Binder was polyvinyl alcohol (PVA, M.W. 22 000, BDH Limited Poole, England) and plasticiser was glycerol (85% PH. EUR, Tamro Vnr 345835).

2.2. Sample preparation

Fig. 1 shows the two routes that were used for preparation of the free-standing and the supported films. The solid content of the slips prepared from each powder was adjusted to 75 wt.% and pH was adjusted to 4 for achieving the electrostatic stabilisation. For break-

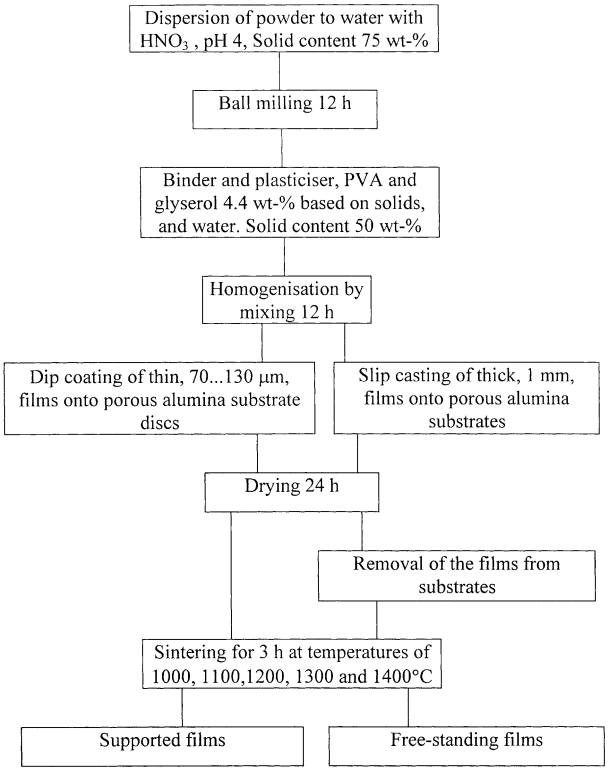

Fig. 1. Preparation procedures for the supported and the free-standing films.

ing possible agglomerates and achieving the complete deflocculation the slips were ball-milled for 12 h. Into defocculated slips PVA–water solution (15 wt.%), glycerol and water were added so that the solid content of 50 wt.% and concentrations of 4.4 wt.% for PVA and glycerol were achieved. The slips were finally homogenised by mixing them for 12 h.

The films were slip cast onto porous alumina substrates. The free-standing films were cast onto the substrate plates aiming to thickness of 1 mm. Shrinkage detached these thick films from the substrate during drying. After 24 h drying at the ambient environment the films were sintered for 3 h at temperatures of 1000, 1100, 1200, 1300 and 1400 °C using heating and cooling rate of 5 °C/min.

For preparation of the supported films discs having diameter of 28 mm were drilled from the substrate plate. The measured pore size and permeability of the discs varied from 1.8 to 2.4 μm and from 1 to 3 m^3/m^2hbar, respectively. The films were dip coated onto these discs with short contact times aiming to thin films. After drying the supported films were sintered together with the free-standing films. The thickness of the sintered, supported films varied from 70 to 130 μm.

2.3. Characterisation methods

The powders were analysed by X-ray fluorescence spectrometry (XRF) in Rautaruukki Steel, Raahe Steel Works, Finland.

Archimedes' method was used for calculation of the density of the samples after sintering. The density and porosity of supported films were calculated by using the mass of the films and the volume of films, calculated from the area of the discs and the measured thickness of the films.

Pore sizes of the free-standing films were measured by mercury porosimetry method. Method is not suitable for thin supported films because of the low pore volume of the film. Therefore, the capillary flow porosimetry was used for the pore size measurement of the supported films. Flow of air through the dry sample was measured first. After that, the sample was impregnated with ethanol. Flow of air through the wet specimen was then measured. The flow through the wet specimen was compared to the flow of the dry specimen at different pressures. The pore diameter, d_{pore}, is related to pressure, dP, as follows:

$$d_{pore} = \frac{4\gamma\cos\theta}{dP} \quad (1)$$

The surface tension of ethanol, 22 mN/m, was used in the calculation. The complete wetting between ethanol and pore walls was assumed. The flow pore size distribution of the sample was obtained by plotting the ratio between the wet flow and the dry flow versus pore diameter.

Scanning electron microscope was used to examine surfaces and cross-sections of the samples. The cross-sectional samples were cast in resin and polished before examination. The grain size was determined from the surface micrographs by measuring at least 100 grains.

Hardness of the free-standing and the supported films was measured by Vickers indentation method with the load of 0.5 kg. The hardness value was calculated as the average of 10 measurements.

Permeability of the films was measured with de-ionised water. The free-standing sample was attached between seals at the bottom of the measuring chamber. The chamber was filled with de-ionised water and pressurised. Pressure was kept steady several minutes and the permeate was collected. The permeability was calculated from the amount of the permeate, the pressure difference, the membrane area, the membrane thickness and the viscosity of water. Permeability of the free-standing films was determined in two steps. The permeability of the substrate without the film and with the film was measured. The pressure drop over the two-layered structure was assumed to consist of the pressure drops of both layers. Since the flux through the substrate and the membrane is same, and the permeability of the substrate is known, the pressure drop over substrate can be calculated. When the pressure drop over the substrate is subtracted from the pressure difference over the whole structure, the pressure drop over membrane is obtained. Since the flux through the membrane was measured and the pressure drop over the membrane was calculated, the permeability of the membrane layer is obtained by using the membrane thickness and the viscosity of water.

3. Results and discussion

3.1. Alumina powder properties

The measured properties of the used alumina powders together with values supplied by manufacturers are listed in Table 1. The measured purity levels were near the values given by the manufacturers. The A 16 SG powder contained the highest amount of impurities. The CR 6 and AKP-30 powders showed similar and low impurity levels. Microscopic examination showed that the particles of A 16 SG powder had irregular shape, whereas the CR 6 and AKP-30 powders had smooth surface morphology. The measured specific surface area was the highest for A16 SG suggesting the presence of fine fraction and irregular shape of particles. CR 6 and AKP-30 had almost same specific surface area indicating the similar primary particle size and distribution. Microscopic examination, particle size and surface area of CR 6 suggest that the powder consists of agglomerates.

Table 1
Properties of the alumina powders

	Alcoa A16 SG	Baikalox CR 6	Sumitomo AKP-30
Phase (manuf.)	α	α > 94%	α
Purity (manuf.)	99.80%	99.99%	99.99%
(measured)	99.57%	99.84%	99.87%
(impurities)	0.122 SiO_2	0.027 Cl	0.036 Na_2O
	0.082 Na_2O	0.022 Na_2O	0.008 Cl
	0.023 CaO	0.007 Fe	0.006 Fe
	0.017 Fe	0.005 K_2O	0.002 CaO
Mean particle size (manuf.)	0.4–0.5 μm	0.55[a] (0.25)[b] μm	0.3–0.5 μm
Specific surface area (manuf.)	8–10 m^2/g	5–7 m^2/g	5–10 m^2/g
(measured)	8.3 m^2/g	6.2 m^2/g	6.7 m^2/g

[a] Mean agglomerate size.
[b] Ultimate particle size.

3.2. Densification and microstructure

The density of supported films was lower than that of the free-standing films as shown in Table 2. The drying shrinkage of the thin films on the substrate is restricted leading to the lower density compared to the thick free-standing films, which are detached from the substrate during drying and can freely shrink in all three directions. The variation in green density of the free-standing films made from different powders indicates differences in packing behaviour during consolidation. The A 16 SG and AKP-30 films had rather dense packing as the result on the complete deflocculation. The free-standing CR 6 film had lower green density, which also suggests that there is agglomerates in the slip. Densification of the free-standing films during isothermal sintering was rather slow until the temperature was raised up to 1300 °C. The isothermal sintering at 1400 °C resulted in almost dense films made from A16 SG and AKP 30. The density of CR 6 film was 3.85 g/cm^3 after sintering for 3 h at 1400 °C. All the porosity left was open. The density of the supported films remained low after sintering at high temperatures. Inaccuracy of the film thickness measurement resulted inlarge scatter on density values and therefore the densification of the supported films was difficult to determine. The density of the supported films was anyway much lower than the density of the films sintered without the substrate. The densification of the supported films will probably occur at the higher temperatures and longer dwell times.

Table 2
Density of the free-standing and the supported films after different sintering cycles

	Density (g/cm^3)		
	A 16 SG Free/supp.	CR 6 Free/supp.	AKP-30 Free/supp.
Green	2.41/n.a.	1.94/n.a.	2.43/n.a.
3 h 1000 °C	2.43/2.02	1.95/1.65	2.50/2.51
3 h 1100 °C	2.51/2.34	2.00/1.76	2.64/2.80
3 h 1200 °C	2.73/2.18	2.10/1.64	2.90/2.67
3 h 1300 °C	3.25/2.16	2.39/1.96	3.47/2.74
3 h 1400 °C	3.79/2.34	2.51/1.93	3.85/2.41

The specific surface area was compared with the fraction of theoretical density for evaluation of the densification mechanism. From Fig. 2 it can be observed that the specific surface area of the A 16 SG and CR 6 compacts decreased without densification at low temperatures indicating neck growth between particles by the surface diffusion mechanism or smoothening of particle surfaces. In temperature ranges from 1000 to 1100C for A 16 SG and 1100 to 1200 °C for CR 6 the densification occurred faster than the specific surface area were reduced. When temperature was further increased, the surface area decreased again rather fast compared to the densification. This difficulty in densification might be due to grain growth or local densification. The local densification has minor effect on the macroscopic volume of the sample. At higher temperatures, 1200 °C and over for A 16 SG and 1300 °C and over for CR 6, the surface area decreased while compact density increased. The compact made from A 16 SG powder and sintered for 3 h at 1400 °C did not reach the theoretical density. The surface area was almost totally lost, but some closed porosity remained on the sample.

The grain size of the supported films was slightly larger compared to the free-standing films as shown in Fig. 3. During the longer casting times of the free-standing films the sedimentation may result in increased amount of smaller particles on the surface of the film. The supported films were dip coated onto the substrate and the casting times were shorter resulting in larger particles at the surface because the sedimentation did not have time to occur. In the films made of CR 6 powder the difference between grain sizes was smaller. The grain growth starts at the temperature around 1200 °C for all the films. The grain size of the supported film made of A 16 SG powder had step-like growth when the sintering temperature was increased from 1200

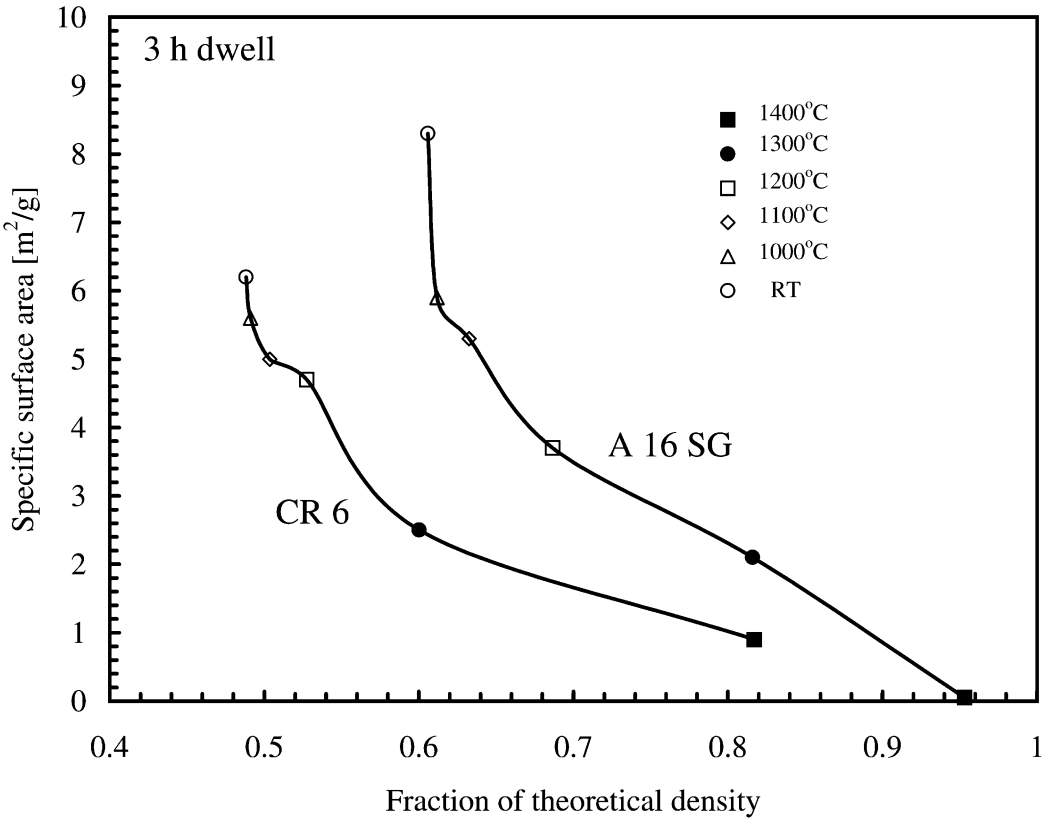

Fig. 2. The specific surface area of the free-standing films versus fraction of theoretical density.

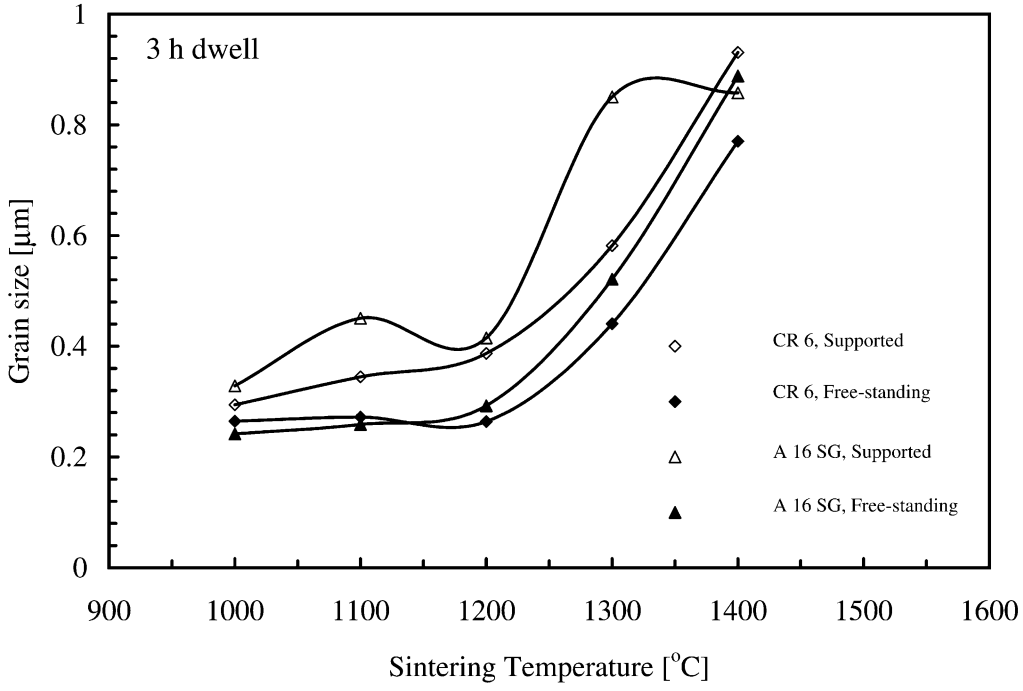

Fig. 3. The grain sizes of the supported and the free-standing films after sintering for 3 h at different temperatures.

to 1300 °C. Although there seems to be a difference in grain growth behaviour, the grain size was same for the supported and the free-standing films after sintering at 1400 °C. In films made of CR 6 powder the grain growth was continuous without steps. The micrographs in Fig. 4 show the surface morphology of films made from A 16 SG. The grain size of the free-standing and supported films is same, but crack like openings between densified areas are present in the supported film.

3.3. Functional properties

The pore sizes of the free-standing films made of A 16 SG powder were slightly smaller than those of the films made of CR 6 powder as shown in Fig. 5. The agglomerates in CR 6 powder resulted looser packing and therefore larger pores. The mean pore sizes of the free-standing films remained almost the same after sintering at different temperatures. The pore size of the free-standing film made from A 16 SG and sintered at 1400 °C could not be measured because of the low open porosity of the sample. The constant pore size suggests that the sintering proceeds mainly by the particle approach and neck growth which reduce the surface area.

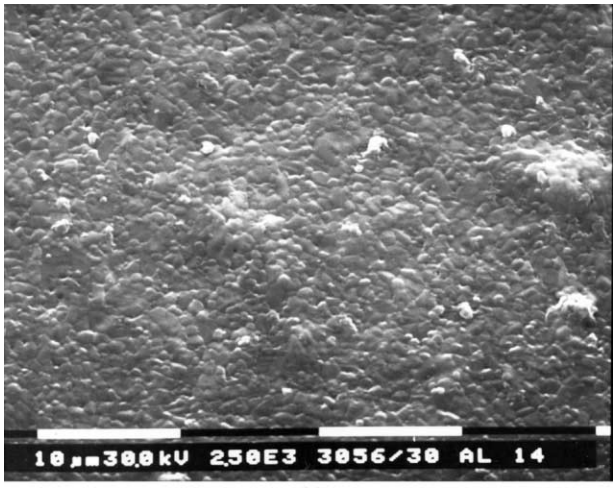

Fig. 4. Surface structure of (a) the free-standing and |(b) the supported A 16 SG films sintered for 3 h at 1400 °C.

The mean pore sizes of the supported films were same as the pore sizes of the free-standing films when sintered at low temperatures, although the characterisation methods were different. The mean pore sizes of the supported films increased significantly after sintering at 1300 and 1400 °C. The pore growth occurred at temperatures where the strong densification of the free-standing films was observed. This suggests pore coarsening instead of densification since the porosity of the supported films decreased only slightly.

The pore size distributions of the supported films remained narrow after sintering at low temperatures. The distributions are presented in Fig. 6 with the ratio, d_5/d_{50}, which describes the width of distribution. The pore size distribution was narrow and monomodal to all the films sintered at the low temperatures. The broadening of pore size distribution was found after sintering at temperatures of 1300 and 1400 °C. The mean flow pore size increased indicating coarsening, but the significant, large pore size fraction also appeared and changed the size distribution to bimodal. The change of distribution from monomodal to bimodal occurred at the sintering temperatures where intense densification should occur. The distribution broadening suggests that the film consist of areas where pores grow faster than in the other areas. Since the densification of the supported films was small, the large pores probably appear around the locally densifying particle agglomerates that was also observed from the surface micrographs. If the pore size coarsening is related only to the grain growth, the shape of the distribution curve should remain constant without presence of the fraction of very large pores. The pore size distributions of the supported A 16 SG and AKP-30 films broadened more clearly than the supported CR 6 film, since free-standing A16 SG and AKP-30 films densified at lower temperatures than the free-standing CR 6 film.

Hardness of the free-standing films increased continuously when the sintering temperature was increased as shown in Table 3. Hardness increase was more intense for the films made from powders that densify at lower temperatures. Hardness increase of the supported films occurred at much higher temperatures. Hardness of the supported A 16 SG film remained at the same level when the sintering temperature was increased from 1200 to 1300 °C. At the same interval the grain size of the film increased suddenly. Sintering seems to favour the grain growth instead of densification for A 16 SG film. Evolution of the hardness of the films made of

AKP-30 powder had similar behaviour as the CR 6 films, only the hardness values were much higher.

The hardness values of the free-standing films were found to be dependent on the density of the film as shown in Fig. 7. The CR 6 films had low hardness values and low density after sintering at low temperatures, but when sintered at higher temperatures where densification occurred, the hardness increased to same level as the hardness of the denser A 16 SG and AKP-30 films. The hardness values fitted into the same density versus hardness curve for all films. When the supported films were sintered at low temperatures, the density

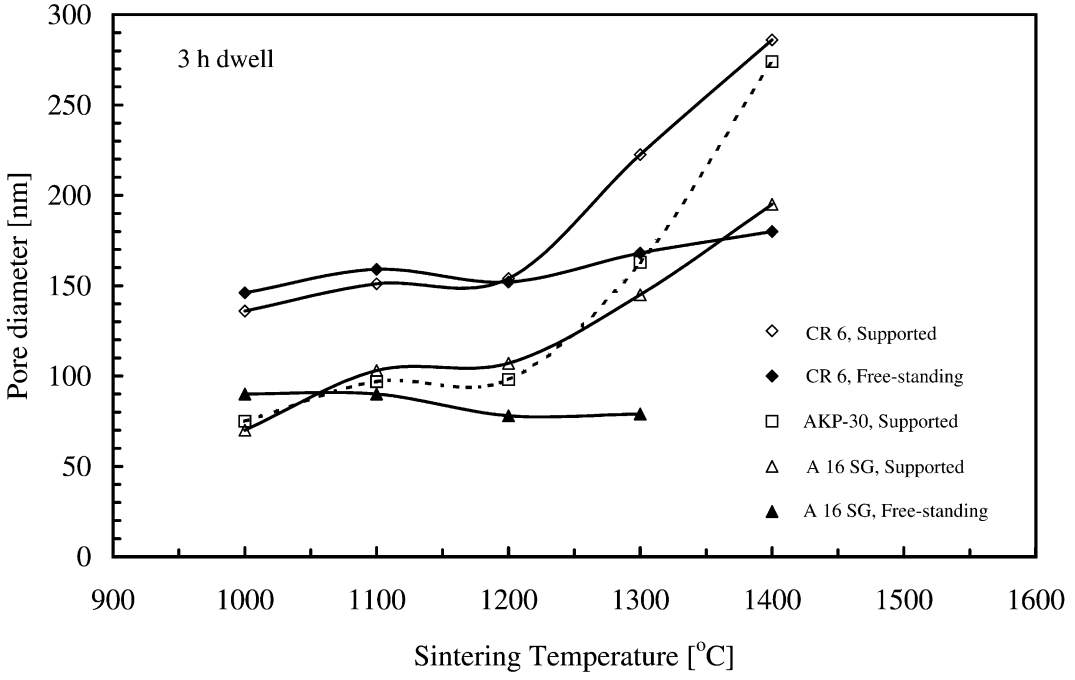

Fig. 5. Mean pore diameter of the free-standing and the supported films after sintering 3 h at different temperatures.

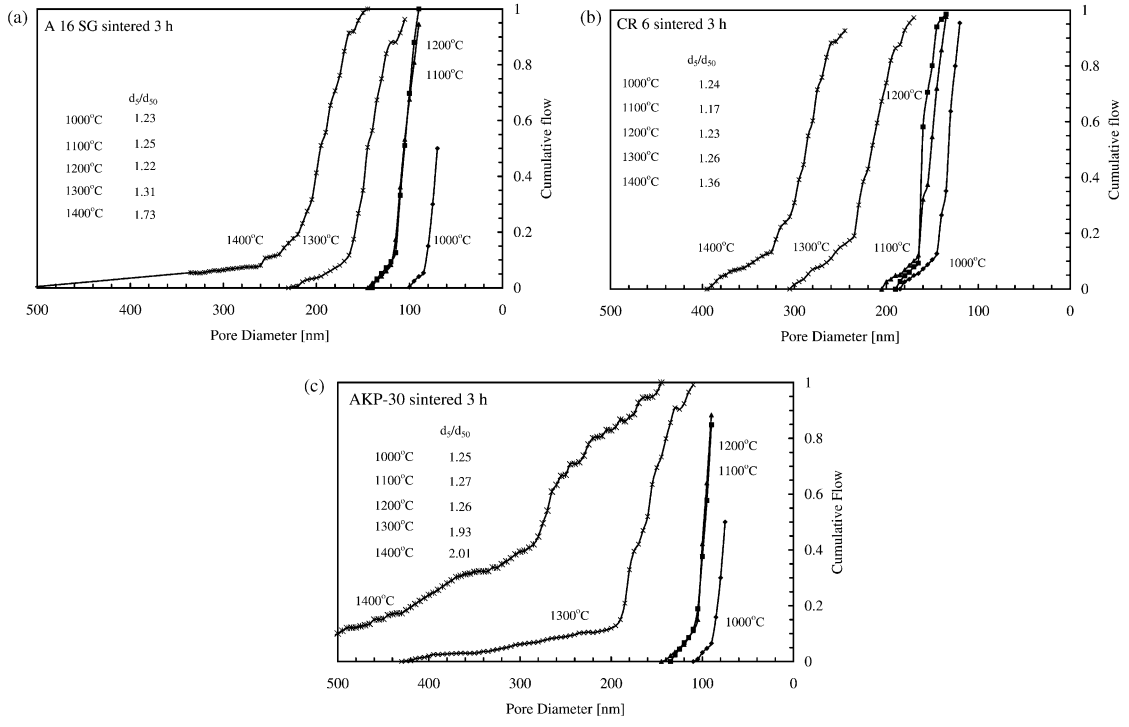

Fig. 6. The flow pore diameter distributions of the supported membranes sintered at different temperatures. The ratio d_{95}/d_{50} is 5% flow of dry sample compared with mean flow. Ratio describes the broadening of the pore size distribution: (a) A16 SG; (b) CR 6; (c) AKP-30.

Table 3
Hardness of the free-standing and the supported films after different sintering cycles

	Hardness (GPa)		
	A 16 SG Free/supp.	CR 6 Free/supp.	AKP-30 Free/supp.
3 h 1000 °C	0.66/0.98	0.22/0.20	1.55/1.02
3 h 1100 °C	1.47/1.49	0.35/0.22	3.23/1.01
3 h 1200 °C	3.44/2.87	0.60/0.24	4.79/1.81
3 h 1300 °C	7.10/2.85	1.54/0.39	7.86/2.75
3 h 1400 °C	14.9/6.11	6.14/2.82	14.8/6.13

increased without having an effect on the hardness. Sintering at higher temperatures increased the hardness, but did not have effect on the density. After sintering at 1400 °C the supported films had much higher hardness values compared to the free-standing films with the same density. Local densification do not affect on the density, but increases the hardness and indicates that the bonds between the densified areas are also strong.

The permeability of the CR 6 films sintered at low temperatures was almost 10 times higher compared with the A 16 SG and AKP-30 films as shown in Fig. 8. The high porosity and the large pore size of the CR 6 films resulted in high permeability. When the sintering temperature of the free-standing A 16 SG film was raised, the permeability decreased continuously due to loss of porosity. The free-standing CR 6 film retained the high permeability value up to the sintering temperature of 1300 °C and above that temperature the permeability decreased due the significant loss of porosity.

Permeability values of the supported films were close to values of the free-standing films made from the same powder after sintering at 1000 °C, indicating rather similar flow channels. When sintering temperature was increased from 1000 to 1200 °C the permeability increased moderately, since there was no significant change of pore size nor porosity. When the sintering temperature was raised to 1300 °C and further to 1400 °C there was more intense increase of permeability especially for the CR 6 film. This increase is related to the coarsening of the pore size and the broadening of the pore size distribution. The A 16 SG and AKP-30 films had permeability increase when the sintering temperature was raised to 1300 °C, but further raise of the temperature did not change the permeability. The pore size of these films increased and porosity remained high, so the reason for steady permeability level after sintering at 1300 and 1400 °C must be in the pore geometry.

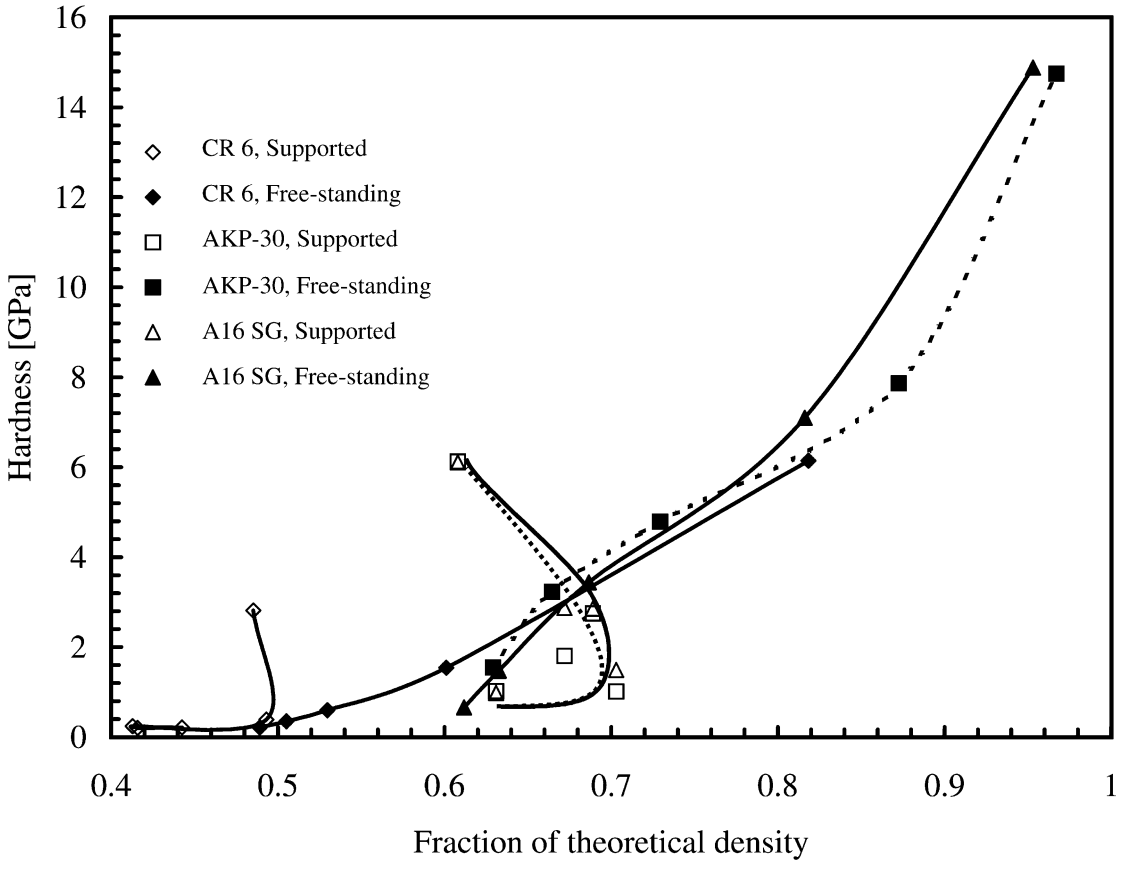

Fig. 7. Hardness of films compared with the fraction of theoretical density.

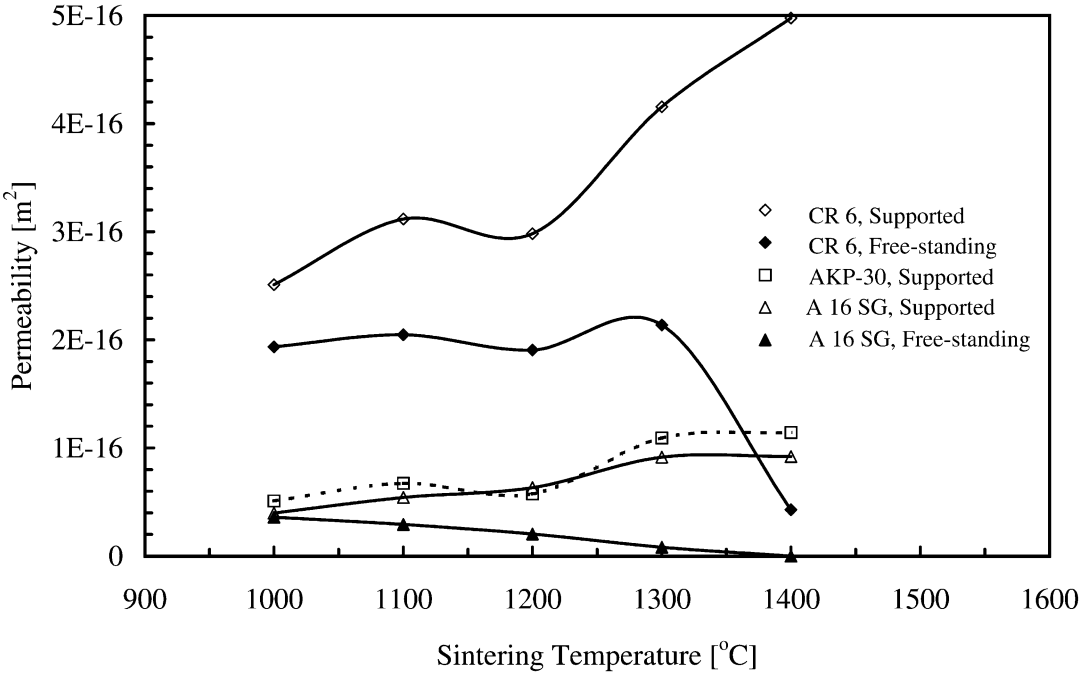

Fig. 8. Permeability of films sintered for 3 h at different temperatures.

The effect of the film properties on the permeability values, K, can be evaluated by using the Kozeny–Carman flow equation.[19]

$$K = \frac{\varepsilon^3}{k_0 k_t S_v^2 (1-\varepsilon)^2} \Rightarrow k_0 k_t = k = \frac{\varepsilon^3}{K S_v^2 (1-\varepsilon)^2} \quad (2)$$

where ε is porosity, k_0 is the pore shape factor, k_t is the tortuosity, defined as square of ratio between the capillary length and the film thickness, S_v is the surface area of compact per volume of dense material. The shape factor k_0 and the tortuosity factor k_t are usually combined to Kozeny–Carman factor k, having frequently used value of 5 to beds packed from particles.

Since the parameters of the Kozeny–Carman equation were measured for the free-standing films, the factor k for these films can be calculated. The calculated values of k for the A 16 SG and CR 6 films are listed in Table 4.

Table 4
Calculated Kozeny–Carman constant, k, values for the free-standing films

	Kozeny–Carman constant k	
	A 16 SG	CR 6
3 h 1000 °C	7.9	6.3
3 h 1100 °C	9.5	4.8
3 h 1200 °C	14.7	4.2
3 h 1300 °C	16.4	3.3
3 h 1400 °C	–	23

The k values for the both films were quite near each other after sintering at 1000 °C, suggesting similar tortuosity and pore shape.

Higher initial k value for the free-standing A16 SG films is result from the broad particle size distribution and dense packing. The k values for the A 16 SG films increased continuously with the sintering temperature, indicating that the flow path is changing more tortuous. The porosity of A 16 SG films decreased rapidly when the sintering temperature was increased, while pore size remained constant, leading to tortuous flow channels as described in A-case in schematic presentation (Fig. 9). The densification may also lead to situation where the Kozeny–Carman flow equation is not valid. If dead end pores appear in the structure, these pores do not take part in the flow through the film. The measured surface area is therefore higher than the surface area of the capillaries participating to the flow, resulting in too high calculated values of the constant k.

The k values for the free-standing CR 6 films decreased when the sintering temperature was increased from 1000 to 1300 °C. The decrease of k suggests the flow channels to come less tortuous as presented in B-case in Fig. 9. After sintering at 1400 °C the k value increased significantly suggesting the formation of tortuous flow channels between dense agglomerates. Due to high initial porosity the closed end pores are not formed into structure and all pores are participating to the flow.

The k factor of the supported films can not be directly calculated, since it is not possible to measure the specific

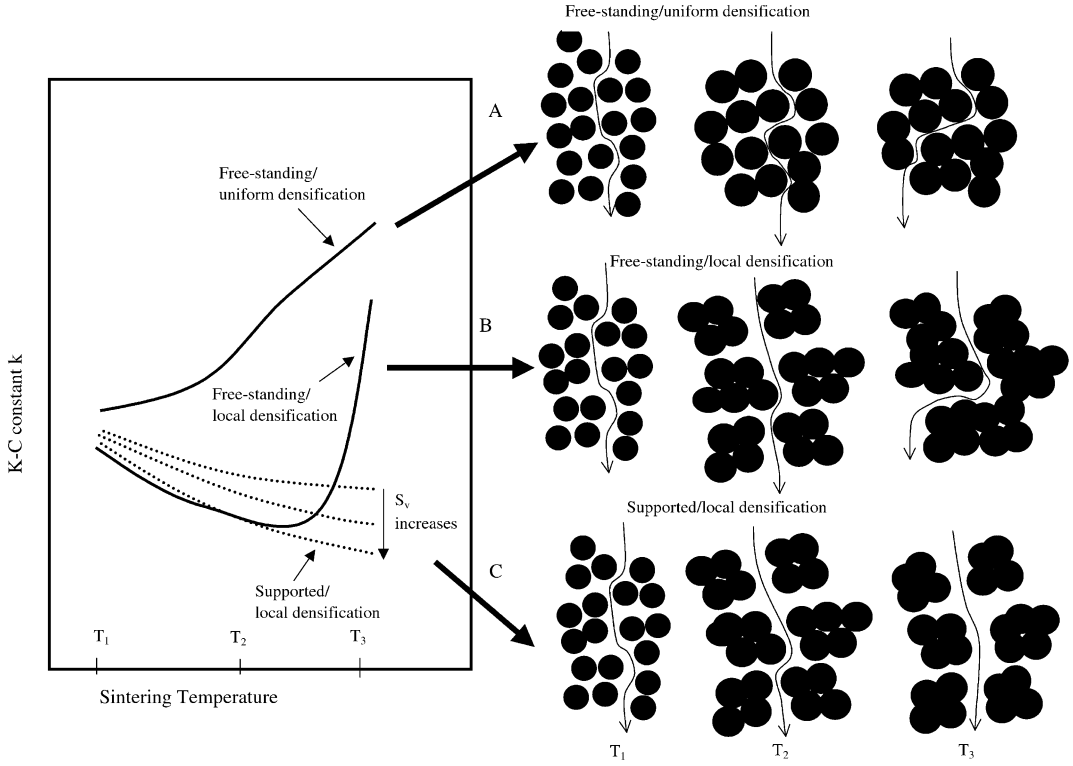

Fig. 9. Evolution of the Kozeny–Carman constant k when increasing the sintering temperature for the free-standing and for the supported films. (A) Uniform densification results in the increase if constant k, since flow bath becomes more tortuous. (B) Local densification of the free-standing film decreases the value of k at low sintering temperatures due to straightening of the flow paths between densified areas. At the high sintering temperatures, the densification occurs also between agglomerates leading again to the tortuous flow paths. (C) The rigid substrate prevents the densification between agglomerates resulting in the continuous decrease of the value of k and straightening of the flow channels between dense agglomerates. The densification of the supported film and the increase of value of k occurs probably at very high sintering temperatures. The evolution of the value of k is based on the estimation that the surface area of the supported film is less than that of the free-standing films. The loss of the surface area for the supported films at different sintering cycles were assumed to be from 1/5 to 1/2 from the loss of surface area for the free standing films after respective sintering cycle.

surface area of film on the substrate. The k factor can be evaluated by estimating the specific surface area of supported film based on the specific surface area of the free-standing film. After sintering cycle the specific surface area of supported film is probably higher than that of free-standing film, due to higher porosity and difficulties in densification. The loss of surface area can be defined as $S_{BET/initial}$–$S_{BET/sintered}$. The loss of specific surface area for the supported films was taken from 1/2 to 1/5 for the loss of surface area for free-standing film. The k factors obtained with these surface area estimations are presented as dotted lines (case C in Fig. 9). The value of k factor for supported films decrease continuously, indicating that the flow channels are straightening when the sintering temperature is raised. The straightening is result from the restriction effect of the substrate. The dense agglomerates can not approach each other, since shrinkage is allowed only one in direction perpendicular to surface. Therefore, much higher sintering temperature is needed before the flow channels transforms tortuous.

4. Conclusions

Sintering at low temperatures, where shrinkage of the free-standing film is small, the narrow pore size distribution of the supported film is retained, but the strengthening of structure is small because of narrow necks between the adjacent particles. The permeability is at the same level for the free-standing and the supported films.

Raising the sintering temperature to range where moderate shrinkage occurs the restricted shrinkage of the supported film leads to the pore coarsening. The neck growth between the particles strengthens the structure, but hardness values are limited to one half of that of the free-standing films. The permeability of the supported films increase due to the pore growth.

Further increase of the sintering temperature results in the strong coarsening of the pore size of the supported films. The pore size distribution is also changing from monomodal to bimodal. A fraction of very coarse pores develops into structure. The rigid substrate

restricts the shrinkage and leads to the local densification. The local densification occurs also in the free-standing films, but in the smaller extent. The effect of local densification on the microstructure, pore properties and hardness of the free-standing films is quite small. The local densification in the supported films leads to dense areas separated by the highly porous regions with large pores. The grain size measurements did not show the faster grain growth in the supported films and the slower densification occurs therefore due to the local densification. The macroscopic densification remains negligible. The permeability of the supported films increase, but functionally the membrane has lost its sharp cut-off value. The hardness of structure increases, but remains about one half of the value of the free-standing film.

Acknowledgements

The Academy of Finland is acknowledged for financing this work, which was carried out within the national research program for Materials Structure Research (MATRA).

References

1. Tiller, F. M. and Tsai, C.-D., Theory of filtration of ceramics: I, slip casting. *J. Am. Ceram. Soc.,* 1986, **69**, 882–887.
2. Philipse, A. P., Bonecamp, B. C. and Veringa, H. J., Colloidal filtration and (simultaneous) sedimentation of alumina and silica suspensions: influence of aggregates. *J. Am. Ceram. Soc.,* 1990, **75**, 2720–2727.
3. van Praag, W., Zapalis, V., Keizer, K., van Ommen, J. G., Ross, J. R. and Burggraaf, A. J., Preparation, modification and microporous structure of alumina and titania ceramic membrane systems. In *Proc 1st Intl. Conf. Inorganic Membranes*, 3–6 July 1989, Montpellier, France, 1990, pp. 397–400.
4. Terpstra, R. A. and Elfrink, J. W., Controlling the pore size of ceramic microfiltration membranes by varying the degree of flocculation of coating suspension. *J. Mater. Sci. Lett.,* 1991, **10**, 1384–1385.
5. Burggraaf, A. J., Keizer, K. and van Hassel, B. A., Ceramic nanostructure materials, membranes and composite layers. *Solid State Ionics,* 1989, **32/33**, 771–782.
6. Larbot, A., Fabre, J. P., Guizart, C. and Cot, L., Inorganic membrane obtained by sol-gel techniques. *J. Membrane Science,* 1988, **39**, 203–213.
7. Lin, Y.-C. and Burggraaf, A. J., Preparation and characterization of high-temperature thermally stable alumina composite membrane. *J. Am. Ceram. Soc.,* 1991, **74**, 219–224.
8. Bordia, R. K. and Raj, R., Sintering behavior of ceramic films constrained by a rigid substrate. *J. Am. Ceram. Soc.,* 1985, **68**, 287–292.
9. Garino, T. J. and Bowen, H. K., Deposition and sintering of particle films on a rigid substrate. *J. Am. Ceram. Soc.,* 1987, **70**, C315–C317.
10. Garino, T. J. and Bowen, H. K., Kinetics of constrained-film sintering. *J. Am. Ceram. Soc.,* 1990, **73**, 251–257.
11. Carroll, D. R. and Rahaman, M. N., An initial stage model for the sintering of constrained polycrystalline thin films. *J. Eur. Ceram. Soc.,* 1994, **14**, 473–479.
12. Zhang, W. and Schneibel, J. H., Calculations of internal stresses during sintering in two dimensions. *J. Am. Ceram. Soc.,* 1996, **79**, 2141–2144.
13. Scherer, G. W. and Garino, T., Viscous sintering on a rigid substrate. *J. Am. Ceram. Soc.,* 1985, **68**, 216–220.
14. Kumar, K.-N. P., Keizer, K., Burggraaf, A. J., Okubo, T. and Nagamoto, H., Textural evolution and phase transformation in titania membranes: Part 2—supported membranes. *J. Mater. Chem.,* 1993, **3**, 1151–1159.
15. Yang, X. and Rahaman, M. N., Thin films by consolidation and sintering of nanocrystalline powders. *J. Eur. Ceram. Soc.,* 1997, **17**, 525–535.
16. Mayadevi, S., Kulkarni, S. S., Patil, A. J., Shinde, M. H., Potdar, H. S., Deshpande, S. B. and Date, S. K., Controlled chemical precipitation of titania for membrane applications—effect of heat treatment and fabrication conditions on its performance. *J. Mater. Sci,* 2000, **35**, 3943–3949.
17. Stech, M., Reynders, P. and Rödel, J., Constrained film sintering of nanocrystalline TiO_2. *J. Am. Ceram. Soc.,* 2000, **83**, 1889–1896.
18. De Hosson, J. T. M., Hooijmans, J. and Popma, R., Sintering behaviour of nanoceramic coatings. *Surface Engineering,* 2000, **16**, 245–249.
19. Carman, P. C., Fluid flow through granular beds. *Trans. Inst. Chem. Eng.,* 1937, **15**, 150.